Progress in Chemical and Biochemical Research

Journal homepage: www.pcbiochemres.com

Original Research Article

Corrosion Inhibition by *Piliostigma Thoningii* Extract on Mild Steel in Acidic Environment: RSM and Molecular Modeling Approach

Asmau Muhammad Sanusi[1,2]*, Bashir Bello Roba[2], Bishir Usman[2]

[1]*Department of Chemistry, Federal College of Education (Tech.), Bichi, Kano State Nigeria*
[2]*Department of Pure and Industrial Chemistry, Faculty of Physical Sciences, Bayero University, Kano, Kano State Nigeria*

ARTICLEINFO

ARTICLE HISTORY

Submitted: 2023-10-13
Revised: 2023-12-17
Accepted: 2024-01-20
Available online: 2024-02-05
Manuscript ID: PCBR-2310-1296
Checked for Plagiarism: Yes
Language Editor: Dr. Fatimah Ramezani
Editor who Approved Publication: Dr. S. L. Sanati, Afsaneh

KEYWORDS

RSM
Inhibition Efficiency
Molecular Modeling
Optimization
Inhibitor
Pilliostigma thoningii

ABSTRACT

The study aimed to optimize the corrosion inhibition performance of an extract from *Pilliostigma thoningii* stem bark on mild steel in 1M HCl environment using Response Surface Methodology (RSM). The optimal inhibitor concentration, temperature, and reaction time were found to be 1.0 g/L, 333 K, and 1 hour, respectively, resulting in an inhibition efficiency of 93.75%. The inhibitor's efficacy was confirmed through various analytical methods, including SEM, FTIR, and UV-Visible spectroscopy. The results suggest that the experimental and predicted data are in reasonable agreement, showing that the quadratic model was the fittest for optimizing the inhibition process. The study identified 33 compounds through GC-MS, with PT-1, PT-2, and PT-3 being the major compounds. Quantum chemical calculations and molecular dynamics simulations further confirmed the effectiveness of the three selected inhibitor molecules, with PT3 being the most effective. The study concludes that *Pilliostigma thoningii* stem bark extract has the potential to be an effective corrosion inhibitor for mild steel in acidic environments.

Citation: Asmau Muhammad Sanusi, Bashir Bello Roba, Bishir Usman. Corrosion Inhibition by *Piliostigma Thoningii* Extract on Mild Steel in Acidic Environment: RSM and Molecular Modeling Approach. Prog. Chem. Biochem. Res., 7(1) (2024)79-99
https://doi.org/10.48309/PCBR.2024.420571.1296
https://www.pcbiochemres.com/article_189760.html

* Corresponding author: Asmau Muhammad Sanusi
E-mail: asmaumuhdsanusi03@gmail.com
Tel number: +2348061510144

GRAPHICAL ABSTRACT

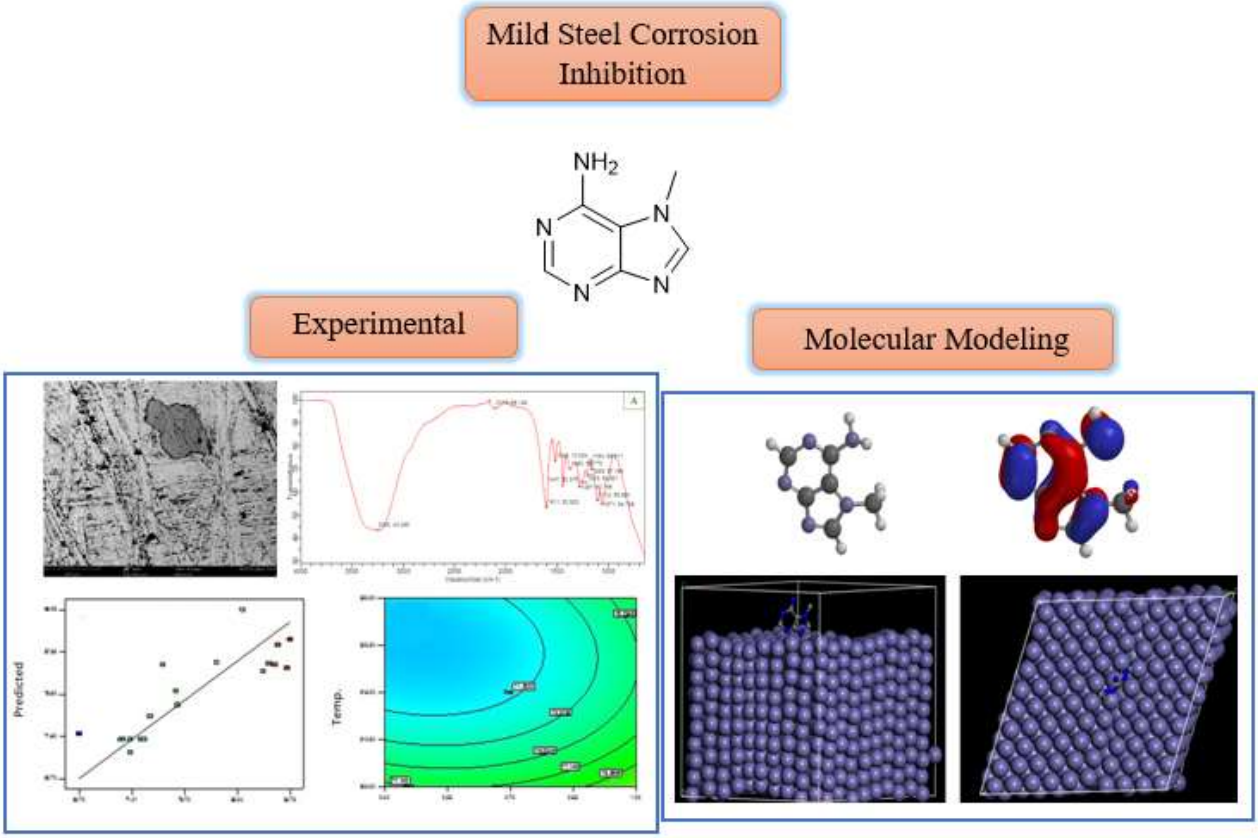

Introduction

Despite its extensive utilization across various industrial sectors, mild steel is highly susceptible to corrosion, leading to significant economic and environmental losses [1, 2]. Corrosion occurs when metals encounter corrosive agents like moisture, acids, bases, salts, oils, and liquid chemicals. This phenomenon leads to considerable economic, environmental, and human losses, emphasizing the critical need to prevent metal corrosion [3]. Corrosion inhibitors are applied to address this issue, and the increasing prominence of using organic compounds is attributed to their ability to form protective films enriched with heteroatoms, including phosphorous, sulfur, nitrogen, and oxygen, on the metal surface. These heteroatoms, along with compounds containing multiple bonds, serve as effective centers for adsorption and corrosion inhibition [4]. Organic inhibitors, particularly those derived from plant extracts, have garnered attention for their cost-effectiveness, biodegradability, renewability, enhanced efficiency, and environmental friendliness. Plant-derived extracts, in particular, have been extensively studied for their corrosion-controlling properties, especially on mild steel [5-7]. One statistical tool employed for studying and resolving corrosion-related problems is the Response Surface Methodology (RSM). This methodology enables researchers to optimize processes involving multiple independent variables that influence a single response variable, such as corrosion rate or inhibition efficiency. By systematically manipulating factors like inhibitor concentration, temperature, and pH, RSM facilitates the identification of optimal conditions for achieving the desired corrosion mitigation outcomes [8,9]. Recent studies have

utilized Response Surface Methodology (RSM) to optimize the corrosion inhibition performance of various inhibitors. For instance, a study conducted by [9] focused on the performance of 2-mercaptobenzimidazole corrosion inhibitor in hydrochloric acid solution during acidizing in the petroleum industry. The study completed the designing of experiments, modeling, and optimization of the corrosion inhibition process based on RSM, examining vital parameters such as inhibitor concentration, temperature, and exposure time at five experimental levels. The developed RSM-based models were highly accurate and reliable, with the percentage of inhibition reaching about 90%. In the same context, the application of Response Surface Methodology led to an 86.78% inhibition efficiency when using *Picralima nitida* leaves extract at a concentration of 1.2 g/L [10]. In another study, Pawpaw leaves extract exhibited 80.29% efficiency in inhibiting mild steel corrosion in HCl medium at a concentration of 1.0 g/L [11]. In a study carried out recently, an Oleoysarcosine was identified as an inhibitor in 0.1M NaCl solution for low carbon steel. The study indicates a high significance linear and quadratic effects of process variables as well as temperature and time interaction effects. The theoretical efficiency predicted by the RSM model was found to be 99.4% and the experimental efficiency was 97.2% [12]. These studies demonstrate the increasing use of RSM in the field of corrosion inhibition, providing valuable insights into the optimization of inhibitor performance and the factors influencing corrosion processes. Theoretical quantum chemical calculations have also proven valuable insight in assessing the corrosion inhibition potential of molecules. Parameters such as frontier molecular orbital energies, energy band gap, dipole moments, global hardness, and softness have been employed to establish correlations between experimental and theoretical data [7,13]. However, it has been observed that relying solely on Density Functional Theory (DFT) calculations may not always yield accurate correlations with experimental results. Therefore, for a comprehensive understanding of interfacial interactions between metallic surfaces and inhibitor molecules, molecular dynamics simulations have emerged as a modern tool. These simulations enable the prediction of the interfacial configurations and adsorption energies of surface-absorbed molecules [14-16].

In this study, we undertake a systematic investigation encompassing optimization techniques, quantum chemical calculations, and molecular dynamic simulations to gain insights into the corrosion-inhibitive performance of an ethanolic extract derived from *Pilliostigma thoningii* (PT) stem bark on mild steel in an acidic environment. The novelty of this work lies in the comprehensive approach to optimize the corrosion inhibition process, including the use of RSM, molecular modeling, and various analytical techniques to validate the inhibitor efficacy, as well as the identification of the major compounds in the extract and their performance through quantum chemical calculations and MD simulations.

Experimental

Materials and methods

The equipment, instrument, and software used in this research consist of the following: threads (ordinary cotton wool thread), Digital Water Bath with temperature ranging from 0-90 °C, Soxhlet extractor (A model of quick fit England with flask capacity of 1000 cm^3), Electrical Analytical Balance with model number FA 2004 weighing up to 250 g maximum and a resolution of 0.1 mg, UV-Visible Spectrophotometer (Perkin Elmer, Lambda 35), Fourier Transformed Infrared Spectroscopy (Agilent Technologies, model carry 630), a combined 7890A Gas Chromatograph system (Agilent 19091-433HP), Scanning Electron Microscope with model PW-100-012 and model NO: 800-07334, DX7 Design Expert 716 software for optimization, and Density Functional

Theory (DFT) using Spartan 14 and Molecular Dynamic Simulation using COMPASS force field (version 2.8).

Preparation of extract

The stem bark of *P. thoningii* sample was collected in Roba town, Dawakin Tofa local government area, Kano State, Nigeria. The plant's identification was conducted at the Herbarium Unit in the Department of Biology at Bayero University Kano, where it was assigned the accession number BUKHAN 469. The sample was subjected to air-drying for a period of 21 days and subsequently crushed into a fine powder. 250 g of the dried powder were placed into 2 liters of 95% ethanol and allowed to sit for 72 hours with occasional agitation.

The mixture was then filtered to yield 24.3 g of the crude extract which was then stored in a clean container in preparation for the corrosion study. To prepare the inhibitor (*P. thoningii* bark extract) for the corrosion inhibition study, 0.2 g of the extract were dissolved in 250 cm^3 of a 1 M HCl solution. The resulting solution was transferred into a 1000 cm^3 volumetric flask and topped up to the mark with a 1M HCl solution. Similarly, other concentrations of the inhibitor (0.4, 0.7, 1.0, and 1.2 g/L) were prepared by dissolving the respective amounts of the inhibitor in the same manner.

Metal preparation

The composition of the mild steel coupons was examined using energy-dispersive X-ray fluorescence (EDXRF) spectroscopy. The EDXRF spectrometer was operated at a voltage of 30 kV and a current of 1 mA for 10 minutes. The mild steel sheet was cut into coupons measuring 2cm x 2cm x 0.36 cm. Before the corrosion process, the coupons were cleaned and polished mechanically with silicon carbide emery paper of grades 120, 400, 800, and 1000 to produce a shiny, polished surface. The coupons were then degreased with acetone to remove oily and organic impurities, and finally washed with distilled water. After drying in the air, the coupons were kept in desiccator.

Gravimetric studies using RSM

A central composite design (CCD) was employed to investigate the combined effects of inhibitor concentration, temperature, and exposure time on the corrosion inhibition efficiency and corrosion rate of mild steel in hydrochloric acid. The CCD is a statistical design method that allows the exploration of the relationships between multiple independent variables and one or more response variables [8]. Table 1 presents the range of the independent variable levels used in the experimental design for the corrosion inhibition.

The experiments were randomly carried out to avoid systematic errors. Total of (20) experiments were conducted, and the results were analyzed with DX7 Design Expert software. The weight loss assessment involved immersing pre-weighed metal coupons in 50 ml of test solution, both with and without an inhibitor, while systematically varying the concentration, temperature, and immersion duration.

Table 1. Variation in experimental design and independent variable levels for inhibiting corrosion in *P. thoningii*

Independent variables	Units	Range				
		Lowest -α	Low -1	Centre 0	High +1	Highest +α
A: Concentration	g/L	0.2	070	0.7	1	1.2
B: Temperature	K	303	318	318	333	333
C: Time	H	0.045	2.5	2.5	4.0	5.02

All weight loss measurements were carried out in hydrochloric acid solutions exposed to aeration, containing various inhibitor concentrations, as described in the experimental setup and outlined in Table 1. At the end of the immersion period, the mild steel specimens were carefully removed from the test solution, subjected to thorough washing with distilled water and acetone, and subsequently dried. The masses of the metal coupon specimens were then measured, and the changes in mass was used in the computation of corrosion rate and inhibition efficiency using Equations (1) and (2), respectively [17,18].

$$R_C = \frac{\Delta w}{AT} \quad (1)$$

Where,

Δw, A, T, and R_C are mass loss (mg), surface area of metal (cm^2), time (h), and corrosion rate ($mgcm^{-2}h^{-1}$), respectively.

$$IE_{WL}\% = \left(1 - \frac{\Delta Winh}{\Delta wblank}\right) x\ 100 \quad (2)$$

Where, $\%IE_{WL}$, $\Delta Winh$, and $\Delta wblank$ are percentage inhibition efficiency (%), mass loss of inhibitor (mg), and mass loss of blank (mg), respectively [19].

Scanning electron microscopy (SEM)

The surface characteristics of the mild steel coupons after immersion in the inhibited and uninhibited acid solutions were assessed using two scanning electron microscopes (SEMs): the PW-100-012 and the model NO 800-07334. Before immersion in the test solutions, the mild steel coupons were polished to a smooth surface. The coupons were then immersed in the test solutions for 5 h at room temperature. After immersion, the coupons were removed, rinsed in distilled water, dried, and studied by SEM. The SEM imageries were taken from the segments of the coupons that provided the most informative data.

Fourier transform infrared spectroscopy

A Fourier transform infrared (FTIR) spectrometer model Carr 630 from Agilent Technologies was used at the Pure and Industrial Chemistry Instrumental Laboratory, Bayero University Kano, to characterize the functional groups of the pure *P. thoningii* bark extract and the corrosion products on the mild steel surface after adsorption. The FTIR spectra were recorded in a region of 400-500 cm^{-1} (wavenumber), and the functional groups were identified by comparing the peak positions with standard values reported in the literature [18,20].

The FTIR analysis provided valuable insights into the chemical composition of the *P. thoningii* bark extract and the corrosion products on the mild steel surface. The spectra showed the presence of various functional groups, such as hydroxyl, carboxylic acid, and amine groups, which are characteristic of the extract's constituents. By comparing the peak positions with standard values, the researchers were able to identify the specific compounds responsible for the extract's corrosion inhibition properties.

UV-Visible spectrophotometry

The optical properties of the *P. thoningii* bark extract were characterized by Perkin Elmer Lambda 35 UV-Visible Spectrometer at the Central Laboratory of Bayero University, Kano. A 0.2 mg sample of the extract was dissolved in 2.5 cm^3 of double-distilled water and the solution was scanned over a wavelength range of 200-600 nm. The stability of the inhibitor molecules was investigated by immersing a mild steel specimen in a solution containing 1 M HCl with an effective concentration of the extract. After 5 h, the specimen was removed, washed with distilled water, and rubbed gently to remove any loose corrosion products. The solution was then examined again by UV-Visible spectroscopy and the results were compared to the spectrum of the pure extract [18,21].

Gas chromatography-mass spectroscopy (GCMS)

The ethanolic extract of *P. thoningii* bark was subjected to GC-MS analysis using a combined 7890A Gas Chromatograph system (Agilent 19091S-433UI). The mass spectra of the

individual components were interpreted using the National Institute of Standards and Technology (NIST) database, which comprises of over 62,000 patterns. The spectrum of each unidentified component was compared to the spectra of the known components in the NIST library to ascertain it. The name, molecular weight, and structure of each component were also determined. The concentrations of the identified compounds were determined by normalizing the peak areas in the GC-MS chromatogram.

Quantum chemical calculation (QCC)

Density functional theory (DFT) calculations were performed to evaluate the quantum chemical descriptors and the structure-activity relationship of the inhibitors (PT-1, PT-2, and PT-3). The structure of the molecules was first drawn with ChemDraw Ultra 12.0 program and their geometry was optimized using DFT (Spartan 14) at the Becke three-parameter Lee-Yang-Parr (B3LYP) level of theory with the 6-311G*(d,p) basis set [22]. Quantum chemical descriptors generated were the energy of the highest occupied molecular orbital (E_{HOMO}), the energy of the lowest unoccupied molecular orbital (E_{LUMO}), dipole moment, Polarizability, energy band gap ($\Delta E = E_{LUMO} - E_{HOMO}$), global electronic chemical potential (μ), chemical softness (σ), chemical hardness (η), and the global electronegativity (χ). The number of transferred electrons (ΔN) was also calculated. The aforementioned descriptors were all computed using appropriate relations (Equations (3-9)) as previously reported [23,24].

$$\Delta E = E_{LUMO} - E_{HOMO} \quad (3)$$

$$\eta = -\frac{1}{2}(E_{HOMO} - E_{LUMO}) \quad (4)$$

$$\sigma = \frac{1}{\eta} = -\left(\frac{2}{E_{HOMO} - E_{LUMO}}\right) \quad (5)$$

$$\mu = \frac{1}{2}(E_{HOMO} + E_{LUMO}) \quad (6)$$

$$\omega = \frac{\mu^2}{2\eta} \quad (7)$$

$$X = \frac{-(E_{HOMO} - E_{LUMO})}{2} \quad (8)$$

The fraction of electrons transferred (ΔN) from the inhibitor to metal were calculated using Equation (9).

$$\Delta N = \frac{X_{Fe} - X_{inh}}{2(\eta_{Fe} + \eta_{inh})} \quad (9)$$

Where, a theoretical value of $X_{Fe} = 7eV$ and $\eta_{Fe} = 0$ was taken from the reference [22]. The results of the DFT calculations can be used to understand how the inhibitor molecule interacts with the metal surface.

Molecular dynamic simulations (MDS)

The molecular dynamic simulation (MDS) was conducted using Material Studio v8.0. In this simulation study, we focused on the Fe (iron) surface.

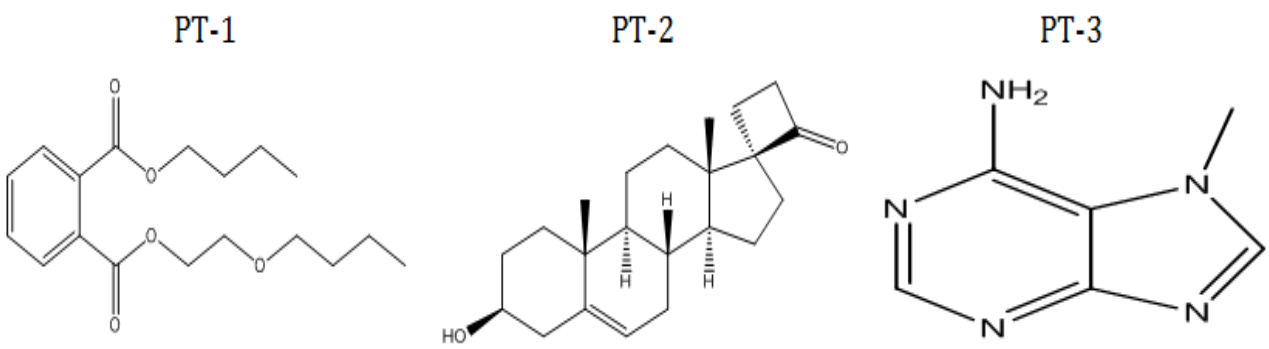

Fig 1. Structural formula of compounds (PT-1, PT-2, and PT-3) from the ethanolic extract of *P. thoningii*

The Fe surface was initially cleaved along the (110) plane, with both the topmost and bottommost layers held fixed. We employed a simulation cubic box measuring 12.5 angstroms in each dimension (12.5 X 12.5 X 12.5) and utilized a fixed number-volume-energy ensemble for the conduct of the molecular dynamics simulation. This simulation aimed to investigate the interaction between the studied inhibitors (PT-1, PT-2, and PT-3) and the Fe (110) surface, known for its higher stabilization energy as reported by [25]. The MD simulation was carried out at a controlled temperature of 298 Kelvin, using the Andersen thermostat and the fixed number-volume-energy ensemble. The simulation employed a time step of 1.0 fs, with a total simulation time of 5 ps. The binding energy between the iron surface and the inhibitor molecules was calculated using Equation (10), as presented:

$$E_{interaction} = E_{Total} - (E_{Fe} + E_{Inh}) \quad (10)$$

Where, E_{total} is the total energy of iron crystal together with the absorbed inhibitor molecules, E_{inh} and E_{Fe} are the free energies of inhibitor molecules and Iron crystal. The binding energy of the inhibitor molecule can be expressed as the negative of the adsorption energy, and it can be described using Equation (11) [26].

$$E_{interaction} = -E_{binding} \quad (11)$$

Results and Discussion

Experimental design and optimization process using RSM

A central composite design (CCD) was employed to conduct 20 experiments to find the optimal conditions for the maximum inhibition efficiency and minimum corrosion rate. The response in the CCD was the percentage inhibition efficiency. Table 2 indicates the RSM experimental design and results, with the concentration of the inhibitor, exposure time, and temperature as the independent variables. This is consistent with the findings of several other authors who have used different extracts to inhibit corrosion [12,27-29]. As presented in Table 2, the experimental results obtained at the optimal conditions are in close agreement with the predicted values. The inhibition efficiency increases to 85.74% at 303 K and decreases to its lowest value of 71.17% at the highest temperature, 343 K. These outcomes are in agreement with those in the literature [27,30]. At the end of the experiments, the experimental results were fitted to a quadratic polynomial design as shown in the following equation:

$$\hat{y} = \hat{\beta}_o + \sum_{i-1}^{k} \beta_i \chi_i + \sum_{i-1}^{k} \beta_{ii} \chi_1^2 + \sum_{i-1}^{k} \sum_{j=1}^{i-1} \beta_{ij} \chi_i \chi_j \quad (12)$$

Where, χ_i and χ_j indicates the design variable and β the turning parameters [8].

The regression coefficients were estimated using the least squares method. The fitted model was then used to predict the inhibition efficiency for any given set of design variables. The outcomes of the RSM analysis show that the inhibitor concentration, exposure time, and temperature all have a significant effect on the inhibition efficiency. The developed model for the inhibition process is illustrated as follows:

$$IE(\%) = +71.17 + 2.44 * A - 2.94 * B + 3.03 * C + 0.74 * A * B - 1.38 * A * C + 4.10 * B * C + 1.86 * A^2 + 3.31 * B^2 + 7.01 * C^2 \quad (13)$$

Mathematical analysis of the corrosion inhibition process

The F-value and P-value confirmed the statistical significance of the regression model, indicating that the model is not likely to have occurred by chance. The analysis of variance (ANOVA) data for the response surface model is provided in Table 3. The P-value is used to assess the significance of a coefficient, with a smaller P-value indicating a more significant coefficient.

Table 2. Experimental result of corrosion inhibition of *P. thoningii* bark extract

Run	A	B	C	Experimental IE [%]	Predicted IE [%]	Error [%]
1	0.70	318.00	2.50	89.90	84.29	0.411
2	1.00	333.00	1.00	93.75	90.44	0.143
3	0.40	333.00	4.00	70.97	68.71	0.066
4	0.40	303.00	1.00	77.70	77.84	0.000
5	0.70	318.00	2.50	93.30	84.90	0.918
6	1.00	303.00	4.00	91.55	85.55	0.469
7	0.40	303.00	4.00	90.69	85.74	0.319
8	0.40	333.00	1.00	92.00	89.36	0.091
9	0.70	318.00	2.50	63.70	72.33	0.622
10	0.70	318.00	2.50	77.50	80.55	0.077
11	1.00	303.00	1.00	75.60	85.49	0.816
12	1.00	333.00	4.00	73.80	75.59	0.027
13	0.70	318.00	2.50	83.30	85.89	0.056
14	0.70	318.00	5.02	87.00	96.09	0.690
15	0.70	292.77	2.50	69.62	71.17	0.001
16	0.70	318.00	0.45	71.00	71.17	0.000
17	1.20	318.00	2.50	72.50	71.17	0.001
18	0.70	318.00	2.50	73.00	71.17	0.002
19	0.70	343.23	2.50	70.00	71.17	0.001
20	0.20	318.00	2.50	72.90	71.17	0.002

A P-value less than 0.05 is generally considered statistically significant. As shown in Table 3, the P-value for the regression model is significant, as indicated by the single star. This suggests that the model terms are statistically significant. Additionally, the linear coefficients (A, B, and C) and the interaction coefficients (A^2, B^2, and C^2) are statistically significant, as their P-values are all less than 0.05.

This means that the concentration of HCl and temperature are correlated with the inhibition efficiency (IE). The lack of fit can be used to assess how well the model fits the experimental data. The model is adequate, as evidenced by the high R-squared value (0.7337) and the significance of the F-test. An R-squared value of more than 0.6 is considered desirable, and higher R-squared values indicate that the predicted values are in good agreement with the experimental data. The predicted R-squared and adjusted R-squared values are both 93.75%, which is in reasonable agreement. The difference between the two values should be less than 20%. Overall, the results suggest that the regression model is statistically significant and provides a good fit to the experimental data. The linear and interaction coefficients for HCl concentration and temperature are statistically significant, indicating that these factors are correlated with the inhibition efficiency.

Surface plots analysis

Figure 2 shows the graphical analysis of the inhibition efficiency of the *P. thoningii* bark extract on mild steel. Figure 2A shows the correlation between actual and predicted inhibition efficiency, which is linear with the data points distributed along the straight line, indicating a good fit for the experimental data. Contour plots were used to make the results of the response surface more visible and understandable. Contour plots are 3D plots created for each pair of factors while keeping the other factors at the middle level [28].

Table 3.ANOVA result for response parameters

Source	SSq	DFr	M.Sq	F-value	*P*-value
Model	1299.66	9	144.41`	3.06	0.0480
A	81.43	1	81.43	1.73	0.2182
B	118.14	1	118.14	2.50	0.1446
C	125.76	1	125.76	2.67	0.1335
A*B	4.41	1	4.41	0.7660	
A*C	15.18	1	15.18	0.5830	
B*C	134.64	1	134.64	0.1220	
A^2	50.04	1	50.04	0.3273	
B^2	158.17	1	158.17	0.0970	
C^2	707.68	1	707.68	0.0031	
Residual	471.62	10	47.16		
Lack of Fit	460.38	5	92.08		
Pure Error	11.24	5	2.25		
Cor Total	1771.28	19			

SSq: Sum of squares; DFr: Degree of freedom; and M.Sq: Mean square

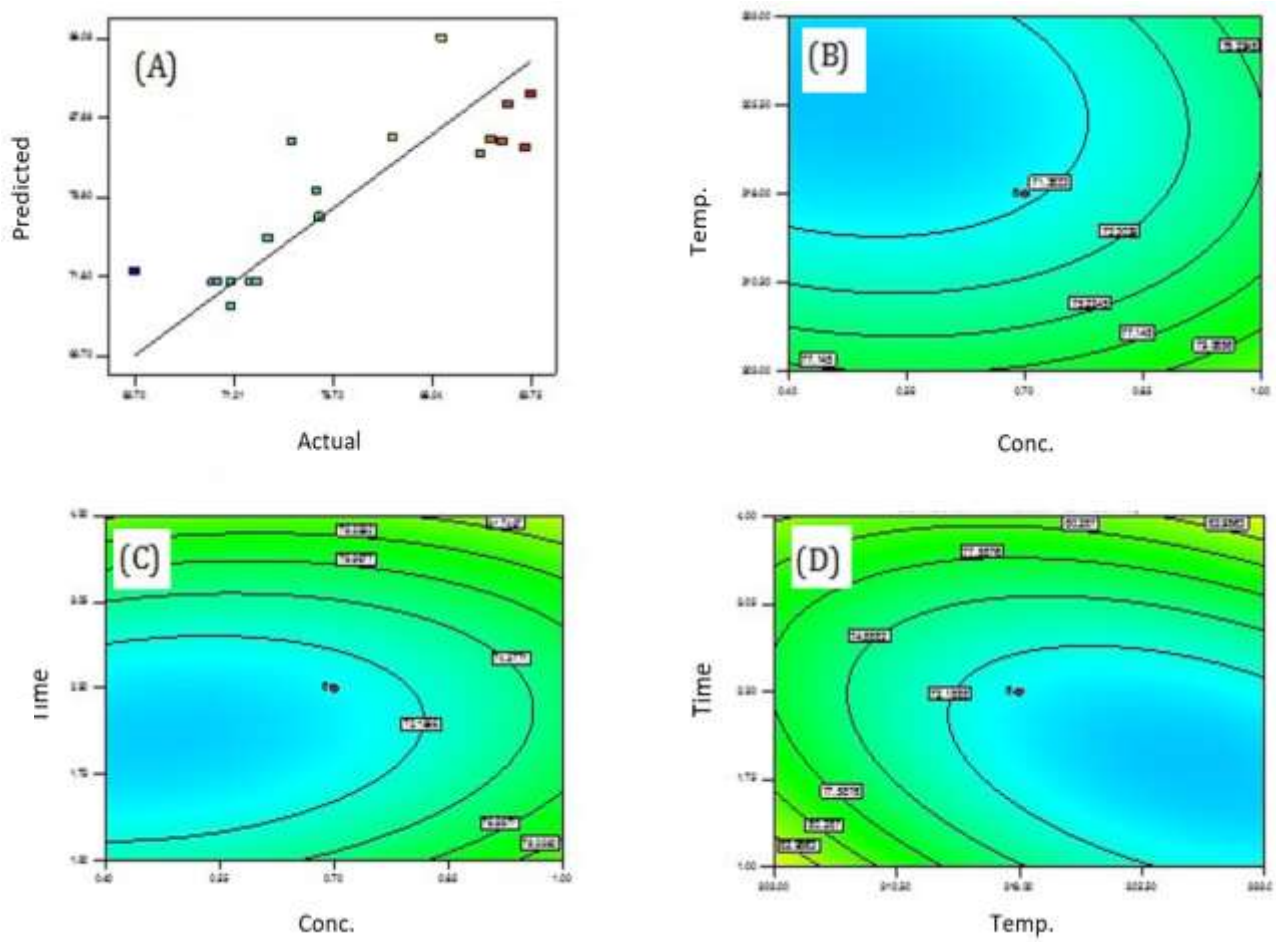

Fig 2.(A) Plot of predicted and actual, (B) effect of inhibitor concentration and temperature, (C) effect of inhibitor concentration and time, and (D) effect of temperature and time, on inhibition efficiency

Figure 2B shows the contour plot of interactions between concentration and temperature. It indicates that the inhibition efficiency increases with increasing concentrations of the inhibitor but decreases with increasing temperature. This is because at higher concentrations, more molecules of the extract are available to block the active sites on the mild steel surface. Figure 2C shows the effect of time on the efficiency of the inhibitor.

The efficiency decreases over time at a constant temperature. At a constant concentration, increasing temperature and time reduce the efficiency. This observation is depicted in Figure 2D, which shows that at higher temperatures and longer contact times between the mild steel and the acid solution, the corrosion rate increases because the rate of dissolution of the metal is higher than the rate of surface coverage. The optimum inhibition efficiency of the PT bark extract is 93.75% at an optimal concentration of 1.0 g/L, a temperature of 333 K, and a time of 1 hour. The rate of inhibition depends on the concentration of the inhibitor, the amount of time that the inhibitor is present, and the type of inhibition.

SEM analysis

Figures 3B and 3C depict the scanning electron microscope (SEM) micrographs of the mild steel surfaces for both the uninhibited and inhibited systems after 6h of exposure at room temperature. Figure 3A depicts the smooth surface of a polished mild steel surface before immersion. The micrograph in Figure 3B shows a very rough surface with numerous corrosion cracks after 6h of immersion in the uninhibited HCl solution. In the presence of the inhibitor, the micrograph in Figure 3C shows a good protective film on the metal surface, which suppresses the corrosion rate. These experimental results clearly show that the inhibition is due to the formation of an insoluble, stable protective film by the adsorption process [18].

FTIR analysis

To further substantiate the adsorption behavior of the inhibitor on the mild steel surface, FTIR spectroscopy was employed. Figure 4B illustrates the FTIR spectrum obtained during the corrosion process when employing an ethanol extract of PT as an inhibitor.The peaks and corresponding frequencies of the FTIR adsorption for both spectra are presented in Table 4. The analysis of the results indicates several notable shifts in peak frequencies: The O-H bond at 3280 cm^{-1} shifted to 3268cm^{-1}, the C=C stretch at 2113 shifted to 2151cm^{-1}, the C=O stretch at 1611 cm^{-1} was shifted to 1618cm^{-1} while the N-H bend at 1525cm^{-1} and shifted to 1559 cm^{-1} and the C-H bend at 1447 cm^{-1} and shifted to 1458 cm^{-1} and also the C-O stretch 1208 cm^{-1} shifted to 1223 cm^{-1}. These frequency shifts indicate a clear interaction for the metal surface and the PT extract inhibitor.

Furthermore, this interaction is visually evident in Figure 4 (A and B), which depict the IR spectra comparison between free mild steel and mild steel with the PT extract inhibitor. These findings align with the results reported in the literature [18,31] confirming the interaction for the metal surface and the PT extract inhibitor.

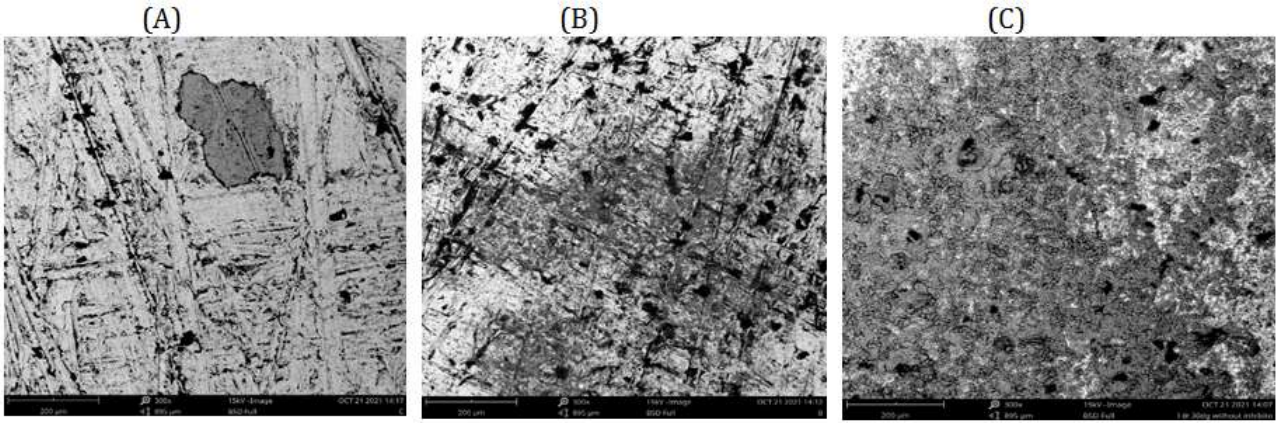

Fig 3. The SEM images of (A) the fresh mild steel, (B) the corroded mild steel, and (C) the mild steel with an inhibitor

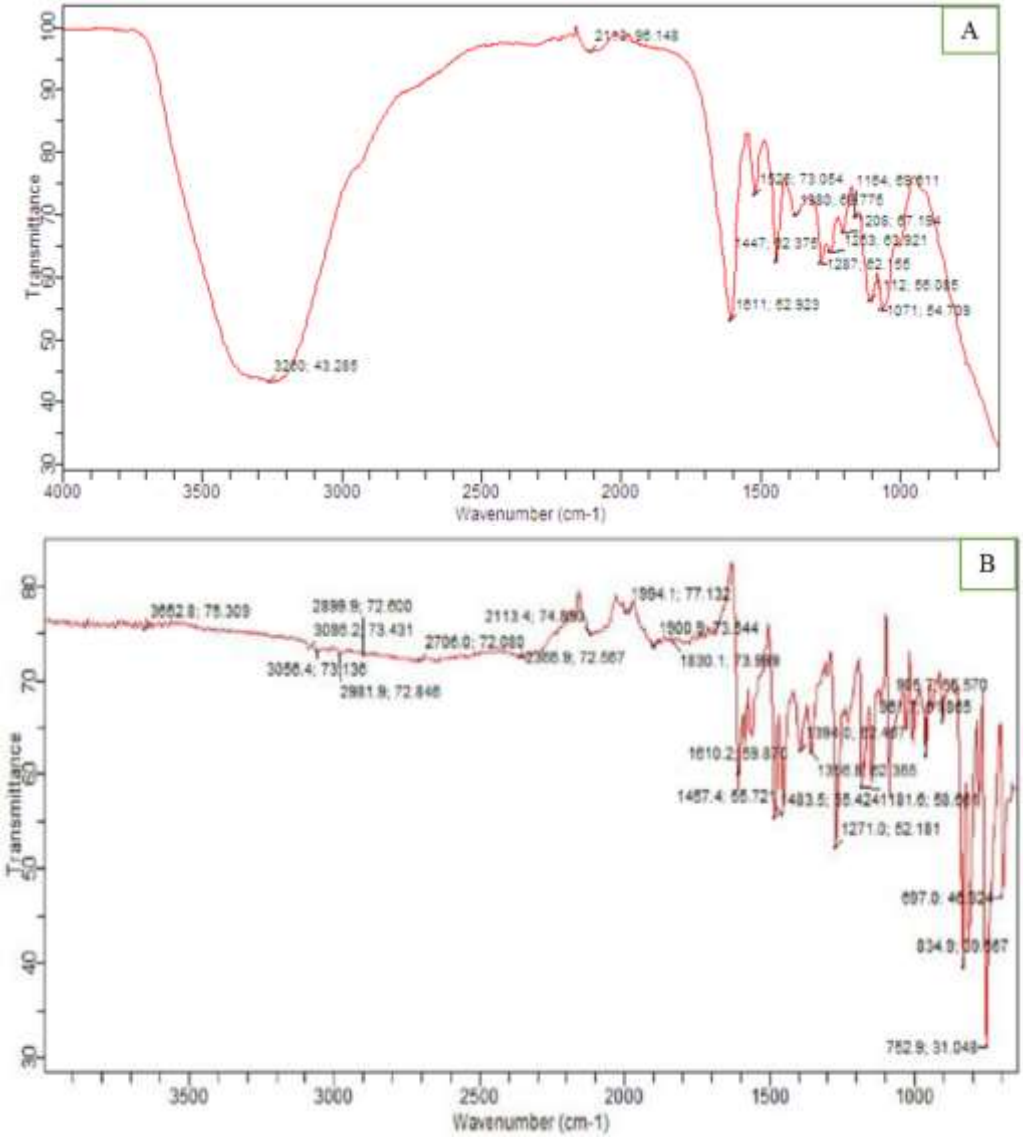

Fig 4.FTIR spectrum of (A) Pure extract of *P. thoningii* bark extract and (B) corrosion product of mild steel in HCl medium with *P. thoningii* bark extract

Table 4. Functional groups assign to the bark extract adsorption and the corrosion product used as an inhibitor

Ethanol	**Extract**		**Corrosion**	**Product**		
Wave No. (cm^{-1})	Height	Assigned functional group	Wave No. (cm^{-1})	Height	Assigned Functional group	Difference (cm^{-1})
3280	43.285	OH H-bonded	3268	92.509	OH H-bonded	12
2113	96.148	C=C stretch	2151	92.381	C=C stretch	38
1611	52.923	C=O amide	1618	89.366	C=O amide	7
1525	73.054	N-H bond	1559	88.794	N-H bond	34
1447	62.375	C-H-CH_3 Bend	1458	88.284	C-H-CH_3 Bend	11
1208	67.194	C-O stretch	1223	87.644	C-O stretch	15

UV-visible spectroscopy

The UV-Visible spectra of the ethanol extract derived from *P. thoningii* bark and the solution containing the mild steel sample immersed in the same extract are depicted in Figure 5 (A and B). A thorough examination of spectrum 'A' reveals the emergence of a peak within the wavelength range of 216.58 nm to 458.90 nm, exhibiting absorbance values of 4.01A and 0.621A, respectively. Figure 5B clearly reveals absorbance peaks occurring at wavelengths ranging from 229.67 nm to 425.21 nm, with absorbance values of 3.70A and 2.61A, respectively.

These spectral changes are attributed to alterations that take place within the extract during the corrosion process. It is more likely that these changes are as a result of the adsorption of bioactive compounds present in the extract. Consequently, this study provides robust evidence supporting the inhibitory properties of the extract solution on mild steel, aligning with the findings of [18].

The UV-Visible spectra analysis provides valuable insights into the interaction between the *P. thoningii* bark extract and the mild steel surface, confirming the adsorption of bioactive compounds onto the metal surface during the corrosion process. This supports the inhibitory properties of the extract and its potential as a green corrosion inhibitor for mild steel in acidic environments.

GC-MS analysis

The gas chromatography-mass spectrometry (GC-MS) chromatogram of the PT extract (Figure 6) displays a total of thirty-three (33) distinct peaks, each corresponding to specific bioactive compounds. These compounds are identified through a comparison of their mass spectral fragmentation patterns with those of known compounds available in the NIST library. The identified chemical constituents are presented in Table 5, which provides details such as peak, retention time (RT), area, ID, and quality for each compound. The main constituents are 1,2-Benzenedicarboxylic acid, 2-butoxyethyl butyl ester- PT-1 (94%), Spiro [androst-5-ene-17,1'-cyclobutan]-2'-one, 3-hydroxy-, (3.beta.,17.beta.)- PT-2 (92%), and 7H-Purin-6-amine, 7-methyl- PT-3 (93%). Three of these compounds PT-1, PT-2, and PT-3 were selected for computational studies to predict their corrosion-inhibitive performance.

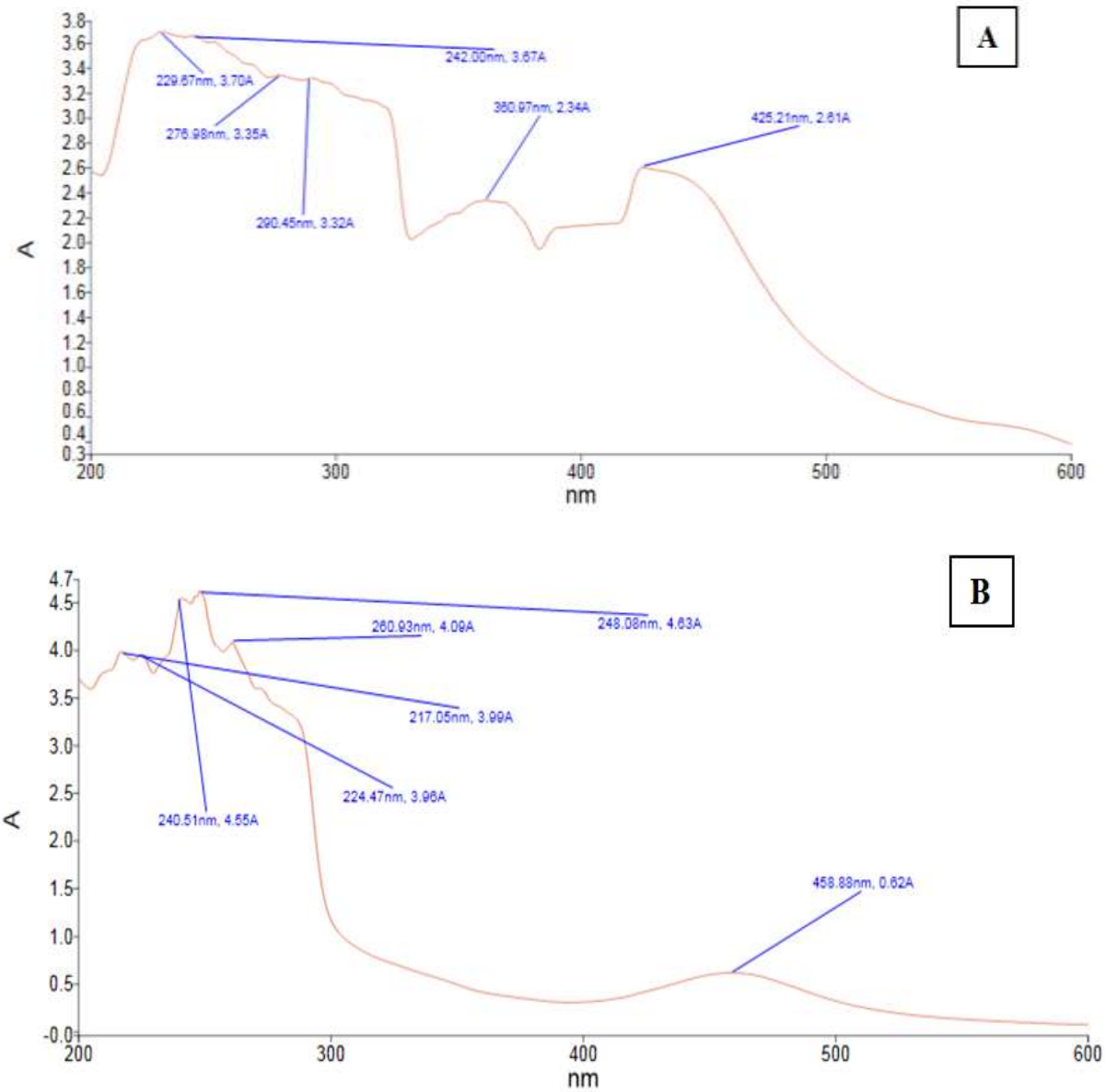

Fig 5.UV-Visible spectra of (A) *P. thoningii* bark extract and (b) bark extract absorbed on mild steel surface

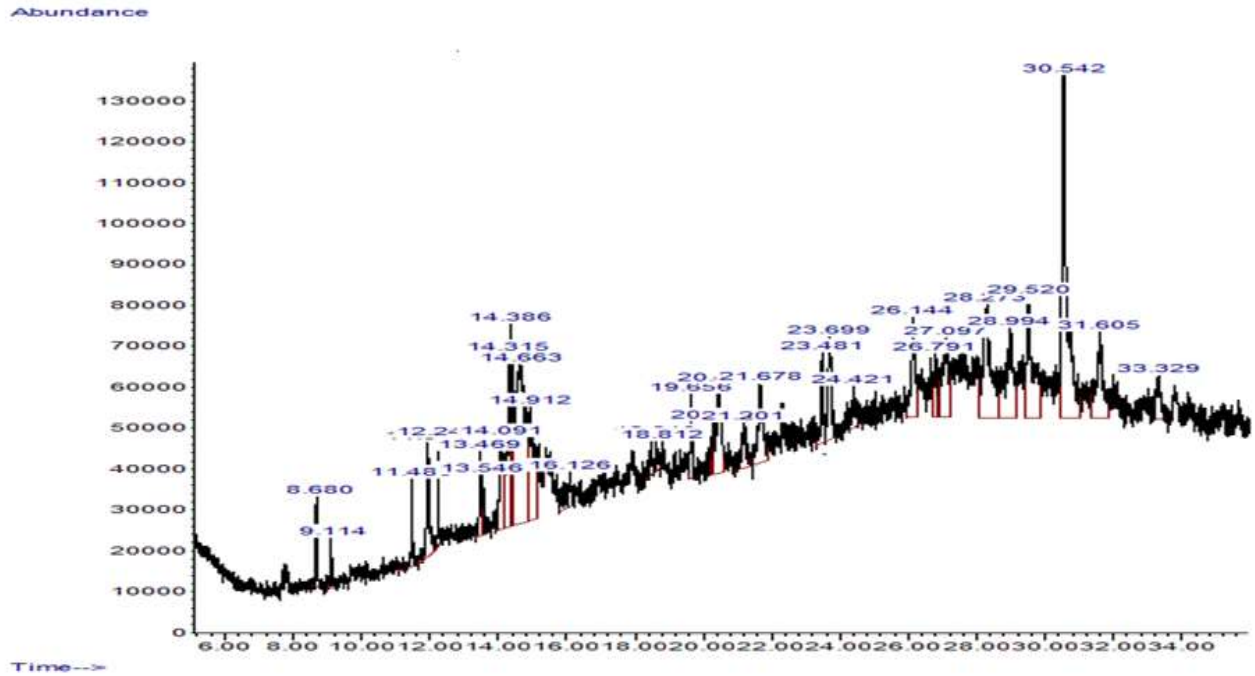

Fig 6.GC-MS chromatogram of *P. thoningii* bark extract

In the present study, the FMO properties of three PT compounds (PT-1, PT-2, and PT-3) were investigated to assess their potential as corrosion inhibitors. The results presented in Table 6 showed that PT-3 had the highest HOMO energy (-7.03) and the lowest LUMO energy (-1.43), suggesting that it is the best electron donor and the most effective corrosion inhibitor of all the three compounds. This is further supported by the fact that PT-3 has the highest dipole moment (7.18), which indicates that it has a greater separation of charge and is more likely to adsorb onto the metal surface.

Overall, the FMO theory and dipole moment measurements suggest that PT-3 is the most effective corrosion inhibitor of the three PT compounds. Molecular descriptors, such as global hardness (η), softness (σ), electrophilicity index (ω), electronegativity index (χ), and fraction of electrons transferred (ΔN), can be used to predict the inhibition efficiency of corrosion inhibitors. According to the hard and soft acid base (HSAB) principle, molecules with low hardness and high softness are more likely to be effective corrosion inhibitors [33]. From the result presented in Table 6, PT-3 has the lowest hardness and highest softness of the three PT compounds, suggesting that it is the best corrosion inhibitor. The electrophilicity index and electronegativity index also support the findings that PT-3 is the best corrosion inhibitor. A higher ω value implies that the molecule is further likely to accept electrons, and a higher χ value implies that the component is more likely to attract electrons from the metal surface [34].

PT-3 has the highest ω and χ values of the three PT compounds. The fraction of electrons transferred(ΔN) from the inhibitor to the metal surface is another important parameter for determining inhibition efficiency. A good corrosion inhibitor should have (ΔN) value greater than zero and less than 3.6 [35]. As can be seen from Table 6, PT-3 has the highest (ΔN) value of all the three PT compounds, indicating that it is more likely to form a strong bond with the metal surface.

Overall, the calculated molecular descriptors suggest that PT-3 is the most effective corrosion inhibitor of the three PT compounds.

Table 5. Parameters deduced from GCMS spectrum of ethanolic extract of *P. thoningii* bark

PK	RT	Area Pct.	Library/ID	Quality
1	8.68	0.8534	Verbenyl angelate, cis-	50
2	9.1138	0.5261	Curlone	38
3	11.486	1.0978	Cyclopentaneundecanoic acid, methyl ester	80
4	11.9507	2.238	Spiro[androst-5-ene-17,1'-cyclobutan]-2'-one, 3-hydroxy-, (3.beta.,17.beta.)-	92
5	12.247	0.929	7H-Purin-6-amine, 7-methyl-	93
6	13.4689	0.9816	cis,cis-7,10,-Hexadecadienal	46
7	13.5464	0.8786	13-Oxabicyclo[10.1.0]tridecane	68
8	14.0906	2.8839	9,12-Octadecadienal	43
9	14.3148	3.6721	9,12-Octadecadienoyl chloride, (Z,Z)-	72
10	14.3858	3.5107	9-Octadecenal	78
11	14.6627	11.9311	.beta.-Sitosterol	38
12	14.9125	4.693	9-Octadecenal	42
13	16.1261	1.5156	Z-12-Tetradecen-1-ol	35
14	18.4641	0.703	Methyl 9,12-heptadecadienoate	49
15	18.6098	0.5884	3-Octyne, 6-methyl-	60
16	18.8121	0.1894	9-Octadecenal	83
17	19.6563	1.2694	isobenzofuran, 1,3-dihydro-1,3-dimethoxy-	38
18	20.2699	0.8702	1,9-Tetradecadiene	55
19	20.4626	3.6617	7-Oxabicyclo[4.1.0]heptane, 1,5-dimethyl-	58
20	21.2011	1.7164	Cyclopentaneethanol, .beta.,2,3-trimethyl-	64
21	21.6777	3.2834	Cyclohexene, 4-(4-ethylcyclohexyl)-1-pentyl-	83
22	23.4807	1.5439	5,9,13-Pentadecatrien-2-one, 6,10,14-trimethyl-, (E,E)-	58
23	23.6993	2.9533	1,2-Cyclopentanediol, 3-methyl-	43
24	24.4206	1.3147	9-Methyl-Z,Z-10,12-hexadecadien-1-ol acetate	46
25	26.1436	3.138	Oxalic acid, isobutyl pentadecyl ester	30
26	26.791	1.0363	9-Octadecenal	60
27	27.0973	3.6251	9-Octadecenal	64
28	28.2733	6.8544	Oxalic acid, isobutyl tetradecyl ester	46
29	28.9939	5.7531	3-Octyne, 6-methyl-	60
30	29.5197	6.1359	(Z)-Tetradec-11-en-1-yl 2,2,3,3,3-pentafluoropropanoate	52
31	30.5423	13.8792	1,2-Benzenedicarboxylic acid, 2-butoxyethyl butyl ester	94
32	31.6047	4.4073	1,11-Dodecadiene	47
33	33.3294	1.366	3-Octyne, 6-methyl-	55

Table 6. Quantum chemical parameters for the studied compounds

Compounds	PT-1	PT-2	PT-3
E-HOMO	-7.03	-6.23	-6.15
E-LUMO	-1.43	-0.54	-0.70
Dipole Moment	1.46	1.06	7.18
ΔE	5.6	5.69	5.45
η	2.8	2.85	2.73
σ	0.357	0.351	0.366
ω	0.381	0.197	9.441
χ	4.23	3.385	3.425
ΔN	0.495	0.634	0.635

Table 7. Optimized structures, E-HOMO, and E-LUMO of the studied compounds

Comp	Optimized structure	E-HOMO	E-LUMO
PT-1			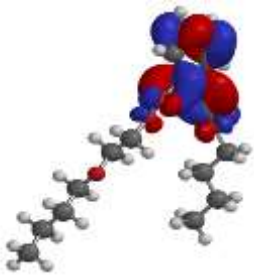
PT-2	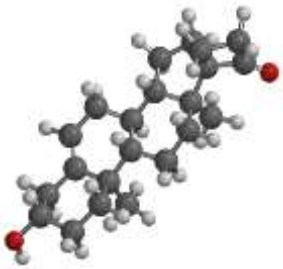	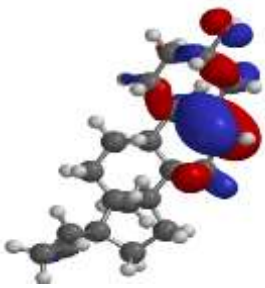	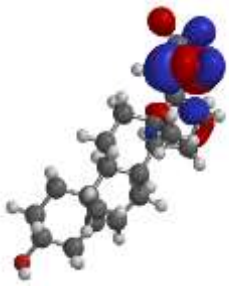
PT-3		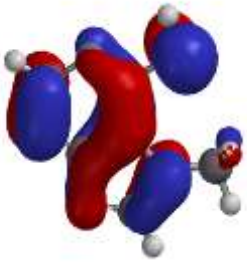	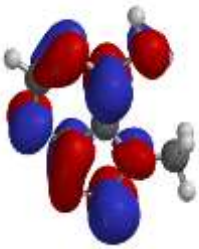

Quantum chemical studies

Frontier molecular orbital (FMO) theory is a useful tool for predicting the reactivity of chemicals and their ability to inhibit the corrosion of metals. The energies of the highest occupied molecular orbital (HOMO) and lowest unoccupied molecular orbital (LUMO) of a molecule provide insights into its electron-donating and electron-accepting abilities, respectively. A higher HOMO energy indicates a greater tendency to donate electrons to the empty d-orbitals of iron, which is beneficial for corrosion inhibition. Conversely, a lower LUMO energy indicates a stronger tendency to accept electrons from the metal, which can promote corrosion [7,22,32].

Table 8. Interaction and binding energies of the inhibitors from molecular dynamic simulation

Comp	$E_{interaction}$ (kcal/mol)	$E_{binding}$ (kcal/mol)
PT1	-347.91	347.91
PT2	-351.01	351.01
PT3	-363.14	363.14

Molecular dynamic simulation

To further understand the mechanism of action and interaction between the three studied compounds and the Fe surface, molecular dynamics (MD) simulations were executed. The system was constructed with the amorphous cell module, and the geometry optimization was conducted until the total energy of the system reached a local minimum on the potential energy surface. The MD simulation was then carried out, and the system was balanced. All three studied inhibitors were studied accordingly. The calculated adsorption energy ($E_{adsorption}$) and binding energy ($E_{binding}$) values are summarized in Table 8. The adsorption configuration of the inhibitor PT-3 over the Fe (1 1 0) surface is depicted in Figure 7. The inhibitor molecule adsorbs in a flat orientation with respect to the iron surface. A chemical-adsorption occurs on Fe surfaces if the binding energy is greater than 100 kcal/mol [25].

As can be seen in Table 6, the calculated binding energy values of the interaction system at 298 K are -347.91, -351.01, and -363.14 kcal/mol for PT-1, PT-2, and PT-3, respectively. This confirms that the adsorption of the molecules onto the metallic surface mainly occurs via chemical adsorption. These results suggest that PT-3 is the most effective corrosion inhibitor of all the three PT compounds, as it adsorb onto the iron surface more spontaneously.

Conclusion

The study has demonstrated that *Pilliostigma thoningii* stem bark extract is a promising green corrosion inhibitor for mild steel in acidic environments. The extract has shown to achieve an optimum inhibition efficiency of 93.75% under optimized conditions. This inhibition performance is attributed to the presence of chemical constituents such as 1,2-Benzenedicarboxylic acid, 2-butoxyethyl butyl ester- PT-1 (94%), Spiro [androst-5-ene-17,1'-cyclobutan]-2'-one, 3-hydroxy-, (3.beta.,17.beta.)- PT-2 (92%), and 7H-Purin-6-amine, 7-methyl- PT-3 (93%). Quantum chemical calculations and molecular dynamics simulations confirmed that the adsorption of the extract molecules onto the metallic surface mainly occurred via chemical adsorption. This suggests that the extract molecules form strong bonds with the metal surface, which inhibits the corrosion process.

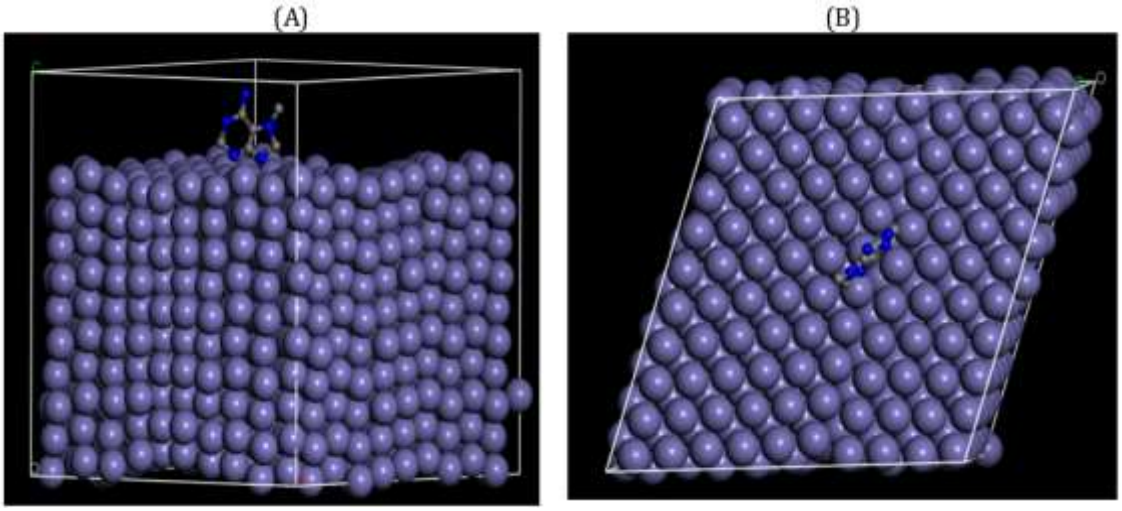

Fig 7. Snapshot (A) side view and (B) top view of inhibitor PT-3 on Fe (1 1 0) surface

The use of *P. thoningii* stem bark extract as a corrosion inhibitor offers several advantages over traditional synthetic inhibitors, as it is a renewable and sustainable resource as well as biodegradable, and it is also non-toxic. In addition, *P. thoningii* stem bark extract is relatively inexpensive and easy to obtain. The findings of this study demonstrate the potential of *P. thoningii* stem bark extract as a viable green corrosion inhibitor for mild steel in acidic environments.

Future research should focus on investigating the long-term corrosion inhibition performance of this plant and developing practical corrosion inhibition formulations based on this extract for industrial applications. Further studies could also explore the use of other plant extracts as corrosion inhibitors and compare their effectiveness with *P. thoningii* stem bark extract. Furthermore, the study could be extended to investigate the corrosion inhibition performance of *P. thoningii* stem bark extract on other metals and alloys in different corrosive environments.

Acknowledgements

The authors are grateful to the physical chemistry units in Bayero University, Kano, and Federal College of Education (Tech.), Bichi, for their technical support and cooperation.

Disclosure statement

The authors declare that they have no conflict of interest.

Funding

The authors declare that no funds, grants, or other support were received during the preparation of this manuscript.

Declarations

Conflict of interest: The authors have no relevant financial or non-financial interests to disclose.
Ethical approval: Not applicable.
Consent to participate: Not applicable.
Consent for publication: Not applicable

ORCID

Asmau Muhammad Sanusi
https://orcid.org/0009-0003-8577-1284
Bashir Bello Roba
*https://orcid.org/*0009-0003-5610-161X
Bishir Usman
https://orcid.org/0000-0002-1738-4368

References

1. Sultana MN, Hasan MF, Islam M. Analysis of mechanical properties of mild steel applying various heat treatment. InProceedings of the International Conference on Mechanical, Industrial and Energy Engineering, Khulna, Bangladesh 2014 Dec (pp. 25-26)., [Google Scholar], [Publisher]
2. Salman TA, Jawad QA, Hussain MA, Al-Amiery AA, Shaker LM, Kadhum AA, Takriff MS. New environmental friendly corrosion inhibitor of mild steel in hydrochloric acid solution: Adsorption and thermal studies, *Cogent Engineering*; 2020 Jan 1; 7(1):1826077. [Crossref], [Google Scholar], [Publisher]
3. Salman TA, Al-Azawi KF, Mohammed IM, Al-Baghdadi SB, Al-Amiery AA, Gaaz TS, Kadhum AA. Experimental studies on inhibition of mild steel corrosion by novel synthesized inhibitor complemented with quantum chemical calculations, *Results in Physics*; 2018 Sep 1; 10:291-6. [Crossref], [Google Scholar], [Publisher]
4. Ahmad Z. Principles of corrosion engineering and corrosion control, *Elsevier*; 2006 Sep 18. [Google Scholar], [Publisher]
5. Rani BE, Basu BB. Green inhibitors for corrosion protection of metals and alloys: an overview, *International Journal of corrosion*; 2012 Jun; 2012. [Crossref], [Google Scholar], [Publisher]
6. Aljeaban NA, Goni LK, Alharbi BG, Jafar Mazumder MA, Ali SA, Chen T, Quraishi MA, Al-Muallem HA. Polymers decorated with functional motifs for mitigation of steel corrosion: an overview, *International Journal of Polymer Science*; 2020 Apr 1; 2020:1-23. [Crossref], [Google Scholar], [Publisher]
7. Abdullahi A, Muhammad A. DFT and molecular dynamic simulation study on the corrosion inhibition of Aluminum by some flavonoids of Guiera Senegalensis leaves, *Algerian Journal of Engineering and Technology*; 2021 Mar 25; 4:66-73. [Crossref], [Google Scholar], [Publisher]
8. Ajeigbe SO, Basar N, Hassan MA, Aziz M. Optimization of corrosion inhibition of essential oils of Alpinia galanga on mild steel using response surface methodology, *ARPN Journal of Engineering and Applied Sciences*; 2017; 12(9):2763-71. [Google Scholar], [Publisher]
9. Khormali A, Ahmadi S. Experimental and modeling analysis on the performance of 2-mercaptobenzimidazole corrosion inhibitor in hydrochloric acid solution during acidizing in the petroleum industry, *Journal of Petroleum Exploration and Production Technology*; 2023 Nov; 13(11):2217-35. [Crossref], [Google Scholar], [Publisher]
10. Ezeugo JN, Onukwuli OD, Omotioma M. Optimization of corrosion inhibition of Picralima nitida leaves extract as green corrosion inhibitor for zinc in 1.0 M HCl, *World News of Natural Sciences*; 2017(15):139-61. [Google Scholar], [Publisher]
11. Omotioma M, Onukwuli OD. Modeling the corrosion inhibition of mild steel in HCl medium with the inhibitor of pawpaw leaves extract, *Portugaliae Electrochimica Acta*; 2016 Sep 26; 34(4):287-94. [Crossref], [Google Scholar], [Publisher]
12. Kaskah SE, Ehrenhaft G, Gollnick J, Fischer CB. Prediction Model for Optimal Efficiency of the Green Corrosion Inhibitor Oleoylsarcosine: Optimization by Statistical Testing of the Relevant Influencing Factors, *Eng*; 2023 Feb 15; 4(1):635-49. [Crossref], [Google Scholar], [Publisher]
13. Mamad DM, Rasul HH, Awla AH, Omer RA. Insight into Corrosion Inhibition Efficiency of Imidazole-Based Molecules: A Quantum Chemical Study. InDoklady Physical Chemistry 2023 Aug; 511(2):125-133. [Crossref], [Google Scholar], [Publisher]

14. Singh A, Ansari KR, Haque J, Dohare P, Lgaz H, Salghi R, Quraishi MA. Effect of electron donating functional groups on corrosion inhibition of mild steel in hydrochloric acid: Experimental and quantum chemical study, *Journal of the Taiwan Institute of Chemical Engineers*; 2018 Jan 1; 82:233-51. [Crossref], [Google Scholar], [Publisher]
15. Khadom AA, Mahmmod AA. Quantum chemical and mathematical statistical calculations of phenyltetrazole derivatives as corrosion inhibitors for mild steel in acidic solution: a theoretical approach, *Results in Engineering*; 2022 Dec 1; 16:100741. [Crossref], [Google Scholar], [Publisher]
16. Bello AU, Uzairu A, Shallangwa GA. Evaluation of Anticorrosion Properties of 1, 2, 4-triazole Derivatives on Steel in Acidic Media using Quantum Chemical Calculation and Molecular Dynamic Simulation Methods, *Portugaliae Electrochimica Acta*; 2020 Sep; 38(6):377-86. [Crossref], [Google Scholar], [Publisher]
17. Odejobi Oludare J, Akinbulumo Olatunde A. Modeling and optimization of the inhibition efficiency of Euphorbia heterophylla extracts based corrosion inhibitor of mild steel corrosion in HCL media using a response surface methodology, *Journal of Chemical Technology and Metallurgy*; 2019; 54(1):217-32. [Google Scholar].
18. I. Jimoh and B. Usman, "Corrosion Inhibition Potential of Ethanol Extract of Acacia nilotica Leaves on Mild Steel in an Acidic Medium," 2021; 39: 105–128. [Publisher]
19. Annon IA, Abbas AS, Al-Azzawi WK, Hanoon MM, Alamiery A, Isahak WN, Kadhum AA. Corrosion inhibition of mild steel in hydrochloric acid environment using thiadiazole derivative: Weight loss, thermodynamics, adsorption and computational investigations, *South African Journal of Chemical Engineering*; 2022 Sep 1; 41(1):244-52. [Google Scholar], [Publisher]
20. Geethamani P, Narmatha M, Dhanalakshmi R, Aejitha S, Kasthuri PK. Corrosion inhibition and adsorption properties of mild steel in 1 M hydrochloric acid medium by expired ambroxol drug, *Journal of Bio-and Tribo-Corrosion*; 2019 Mar; 5:1-8. [Crossref], [Google Scholar], [Publisher]
21. Fergachi O, Benhiba F, Rbaa M, Touir R, Ouakki M, Galai M, Lakhrissi B, Oudda H, Touhami ME. Experimental and Theoretical Study of Corrosion Inhibition of Mild Steel in 1.0 M HCl Medium by 2 (-4 (hloro phenyl-1H-benzo [d] imidazol)-1-yl) phenyl) methanone, *Materials Research*; 2018 Dec 6; 21. [Crossref], [Google Scholar], [Publisher]
22. Umar BA, Uzairu A. In-silico approach to understand the inhibition of corrosion by some potent triazole derivatives of pyrimidine for steel, *SN Applied Sciences*; 2019 Nov; 1:1-0. [Crossref], [Google Scholar], [Publisher]
23. Saha SK, Ghosh P, Hens A, Murmu NC, Banerjee P. Density functional theory and molecular dynamics simulation study on corrosion inhibition performance of mild steel by mercapto-quinoline Schiff base corrosion inhibitor, *Physica E: Low-dimensional systems and nanostructures*; 2015 Feb 1; 66:332-41. [Crossref], [Google Scholar], [Publisher]
24. Musa AY, Jalgham RT, Mohamad AB. Molecular dynamic and quantum chemical calculations for phthalazine derivatives as corrosion inhibitors of mild steel in 1 M HCl, *Corrosion Science*; 2012 Mar 1; 56:176-83. [Crossref], [Google Scholar], [Publisher]
25. Khaled KF. Molecular simulation, quantum chemical calculations and electrochemical studies for inhibition of mild steel by triazoles, *Electrochimica Acta*; 2008 Mar 20; 53(9):3484-92. [Crossref], [Google Scholar], [Publisher]

26. Saha SK, Banerjee P. A theoretical approach to understand the inhibition mechanism of steel corrosion with two aminobenzonitrile inhibitors, *RSC advances*; 2015; 5(87):71120-30. [Crossref], [Google Scholar], [Publisher]
27. Ajeigbe SO, Basar N, Hassan MA, Aziz M. Optimization of corrosion inhibition of essential oils of Alpinia galanga on mild steel using response surface methodology, *ARPN Journal of Engineering and Applied Sciences*; 2017; 12(9):2763-71.[Google Scholar].
28. Kumari P, Lavanya M. Optimization of Inhibition Efficiency of a Schiff Base on Mild Steel in Acid Medium: Electrochemical and RSM Approach, *Journal of Bio-and Tribo-Corrosion*; 2021 Sep; 7(3):110. [Crossref], [Google Scholar], [Publisher]
29. Sanusi AM, Muhammad RA, Sanusi AM, Roba BB, Usman B. Application of response surface methodology using central composite design for the evaluation of corrosion inhibition performance of Pilliostigma thoningii on mild steel in acidic media, *Bayero Journal of Pure and Applied Sciences*; 2022 Jul 3; 13(1):230-7. [Google Scholar], [Publisher]
30. El-Shamy AM, El-Hadek MA, Nassef AE, El-Bindary RA. Optimization of the influencing variables on the corrosion property of steel alloy 4130 in 3.5 wt.% NaCl solution, *Journal of Chemistry*; 2020 Apr 14; 2020. [Crossref], [Google Scholar], [Publisher]
31. Emembolu LN, Onukwuli OD, Okafor VN. Characterization and optimization study of Epiphyllum oxypetalum extract as corrosion inhibitor for mild steel in 3 M H2SO4 solutions, *World Scientific News*; 2020(145):256-73. [Google Scholar], [Publisher]
32. Awe FE, Idris SO, Abdulwahab M, Oguzie EE. Theoretical and experimental inhibitive properties of mild steel in HCl by ethanolic extract of Boscia senegalensis, *Cogent Chemistry*; 2015 Dec 31; 1(1):1112676. [Crossref], [Google Scholar], [Publisher]
33. Khaled KF, Amin MA. Computational and electrochemical investigation for corrosion inhibition of nickel in molar nitric acid by piperidines, *Journal of Applied Electrochemistry*; 2008 Nov; 38:1609-21. [Crossref], [Google Scholar], [Publisher]
34. Wazzan NA, Mahgoub FM. DFT calculations for corrosion inhibition of ferrous alloys by pyrazolopyrimidine derivatives, *Open Journal of Physical Chemistry*; 2014 Jan 29; 4(01):6-14. [Crossref], [Google Scholar], [Publisher]
35. Gao G, Liang C. Electrochemical and DFT studies of β-amino-alcohols as corrosion inhibitors for brass, *Electrochimica Acta*; 2007 Mar 20; 52(13):4554-9. [Crossref], [Google Scholar], [Publisher]